Novel photoactive hyperbranched poly(aryl ether)s containing azobenzene chromophores for optical storage

Xingbo Chen,[a] Yunhe Zhang,[a] Baijun Liu,[a] Jingjing Zhang,[a] Hui Wang,[a] Wenyi Zhang,[b] Qidai Chen,[b] Songhao Pei[c] and Zhenhua Jiang*[a]

Received 9th May 2008, Accepted 6th August 2008
First published as an Advance Article on the web 23rd September 2008
DOI: 10.1039/b807956k

Two novel hyperbranched poly (aryl ether)s with azobenzene moieties in both the main chain and side chain of the branched arms were prepared by using $B_3 + A_2$ methodology *via* a nucleophilic aromatic substitution polycondensation. Structures of the hyperbranched poly (aryl ether)s with azobenzene moieties (azo-HPAEs) were characterized by means of IR, UV-visible, ^{1}H NMR spectroscopy, and XRD. It is shown that both the azo-HPAEs exhibit high glass transition temperatures (T_g), excellent thermal stability and homogeneous photochromic behavior. By exposing their spin-coating films to an interference pattern of laser beam, both the azo-HPAEs could be used for rapid (within 30 s) fabrication of surface-relief gratings (SRGs). The obtained SRGs present no shape changes even at temperatures up to 200 °C. Especially, the azo-HPAE with azobenzene moieties in the side chain shows larger photoinduced birefringence intensity and better reversible optical storage than the one with azobenzene moieties in the main chain upon irradiation with 532 nm Nd:YAG laser. The novel azo-PAEs are photoactive to UV light (355 nm), making them potentially useful for high density information storage.

Introduction

Polymers bearing azobenzene moieties (azo-polymers) have been considered as promising materials for optical data storage, optical switches, electro-optical (EO) modulators, and in other electro-optic areas[1–5] because of the unique reversible photoisomerization between the *trans* and *cis* isomers and an orientational distribution perpendicular to the direction of the polarization of the incident laser beam of the azobenzene chromophore. The photoinduced isomerization can cause significant bulk, surface property variation and polarity of the polymers, such as photoinduced phase transition, photoinduced surface-relief gratings (SRGs), and photoinduced birefringence.[6–11] For decades, research efforts to explore new azo-polymers have predominantly focused on the linear azo-polymers with side-chain or main-chain architectures.[12–15] More recently, dendritic polymers containing azobenzene units have attracted considerable attention and have been intensively investigated.[16–18] The dendrimers are designed to bear azobenzene chromophores in the exterior and interior or throughout the dendritic architecture. Those azo-dendrimers have exhibited some fascinating properties, such as harvesting low-energy photons and improved nonlinear optical properties. In contrast to the intensive study on the azo-dendrimers, only a few hyperbranched azo-polymers have been synthesized and studied.[19,20] The incorporation of azo moieties into hyperbranched polymers could significantly enlarge their potential applications due to their ease of preparation.

There is a continuous demand for high-performance polymers as optical and electronic devices for use in a harsh environment. However, most polymeric materials studied for optical storage were based on aliphatic backbones, which usually had poor thermal stability and low T_g values.[17,20,21] Poly(aryl ether)s (PAEs) are a family of high-performance engineering thermoplastics with excellent thermal, mechanical and electrical properties. Functionalized poly(aryl ether)s have been widely studied as proton-exchange membranes (PEMs), light-emitting materials and optical materials, and some of them exhibited many attractive properties.[22–24] In comparison with the linear poly(aryl ether)s, hyperbranched poly(aryl ether)s (HPAEs) possess a highly branched structure and good thermal properties. To the best of our knowledge, no azobenzene-functionalized HPAEs as optical storage materials have been reported so far. The presence of highly branched structure may facilitate *trans–cis* isomerization of azo groups. Thus the combination of the HPAEs backbone with photoactive azo groups could provide a new approach to develop novel high-performance materials with optical properties. Following this guidance, two kinds of HPAEs with different azobenzene chromophore substitutes located in both the main chain and side chain of the branched arms (Scheme 1) were synthesized by using $B_3 + A_2$ methodology *via* a nucleophilic aromatic substitution polycondensation, and their thermal property, photoisomerization, formation of SRGs and photoinduced birefringence were fully investigated. The novel azo-PAEs are also photoactive to short wavelength light, making it possible to fabricate their SRGs by using a UV laser beam of 355 nm.

[a]*Alan G. MacDiarmid Institute, Jilin University, Changchun, 130012, China. E-mail: jiangzhenhua@jlu.edu.cn; Fax: +86 431-85168886; Tel: +86 431-85168886*
[b]*State Key Lab on Integrated Optoelectronics, College of Electronic Science and Engineering, Jilin University, Changchun, 130012, China*
[c]*College of Physics, Jilin University, Changchun, 130012, China*

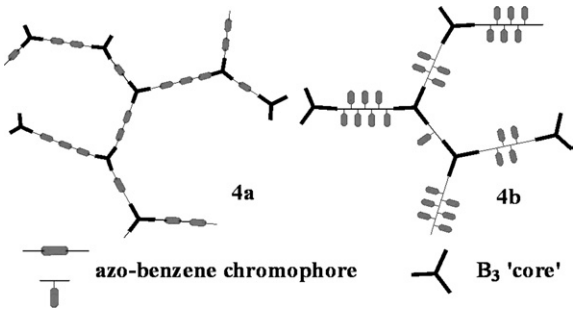

Scheme 1 Schematic of azo-HPAEs **4a** and **4b**.

Experimental

Materials

Phloroglucinol and 2,6-difluorobenzoyl chloride were purchased from Aldrich. 4,4′-Difluorbenzophenone and 4,4′-dichlorodiphenyl sulfone were purchased from Changzhou Huashan Chemical Co., Ltd (China) and were purified before use. Phenol was purchased from Beijing Chemical Factory. 4,4′-Diaminodiphenylsulfone (DDS) and 4,4′-isopropylidenediphenol (BPA) were purchased from Shanghai Chemical Factory. Anhydrous potassium carbonate (K_2CO_3) was dried at 120 °C for 24 h before being used for polymerization. All other chemicals were obtained from commercial sources and used as received.

Measurements

Gel permeation chromatograph (GPC) was carried out using a Waters 410 instrument with *N*,*N*-dimethylformamide (DMF) as an eluent and polystyrene as calibration standard. Inherent viscosity was determined on an Ubbelohde viscometer in a thermostatic container with a polymer concentration of 0.5 g dL^{-1} in DMF at 25 °C. IR spectra (KBr pellet) were recorded on a Nicolet Impact 410FTIR spectrophotometer. ^1H and ^{13}C NMR spectra were recorded on a Bruker 510 (^1H, 500 MHz; ^{13}C, 125 MHz) instrument using dimethysulfoxide-d_6 (DMSO-d_6) or $CDCl_3$ as solvent. Thermogravimetric analyses were performed on a PerkinElmer Pyris 1 TGA under a nitrogen flow (100 mL min^{-1}) at a heating rate of 10 °C min^{-1}. Glass transition temperatures (T_g) were determined using a DSC (Mettler Toledo DSC821°) instrument at a heating rate of 20 °C min^{-1} and under a nitrogen flow of 200 mL min^{-1}. The reported T_g value was recorded from the second scan after first heating and quenching. Wide-angle X-ray diffraction (WAXD) measurements were made using a Siemens D5005 diffractometer equipped with a CuK_α radiation source at room temperature. The powder sample was multiplied to increase the intensity in the range of 4–40° (2θ). Polarized optical microscopy (POM) observation was performed on a Leica DLMP with a Linkam THMSE 600 hot stage. UV-visible absorption spectra were recorded on a UV2501-PC spectrophotometer in DMF solution at room temperature.

Synthesis

1,3,5-Tris(4-(4-fluorobenzoyl)phenoxy)benzene (monomer 1, Scheme 2a). Phloroglucinol (10.08 g, 0.08 mol), 4,4′-difluorobenzophenone (210 g, 1.12 mol), K_2CO_3 (20 g, 0.15 mol), *N*-methyl-2-pyrrolidone (NMP) (500 mL) and toluene (130 mL) were placed in a 1000 mL three-necked flask fitted with a nitrogen inlet, a thermometer, a Dean–Stark trap and a mechanical stirrer, and the apparatus was purged with nitrogen. The reaction mixture was refluxed at 140–160 °C for 6 h to ensure complete dehydration. After removing the toluene, the reaction mixture was heated to 170–190 °C for 4 h under a nitrogen atmosphere. The final solution was poured into a mixture of deionized water (2 L) with hydrochloric acid (50 mL) under vigorous stirring, and then the precipitate was collected by filtration. The crude product was washed with deionized water and ethanol to give a white powder (30% yield). m.p. 131 °C; *m*/*z* (MALDI-TOF): 721 ($C_{45}H_{27}F_3O_6$ requires 720.18); ν_{max}/cm^{-1} 1656 (–C=O), 1238 (–O–); δ_H (500 MHz; $CDCl_3$, Me_4Si): 6.61 (1H, s, ArH), 7.13 (2H, d, $J = 8.7$ Hz, ArH), 7.17 (2H, t, $J = 8.6$ Hz, ArH), 7.81 (2H, m, ArH), 7.83 (2H, m, ArH).

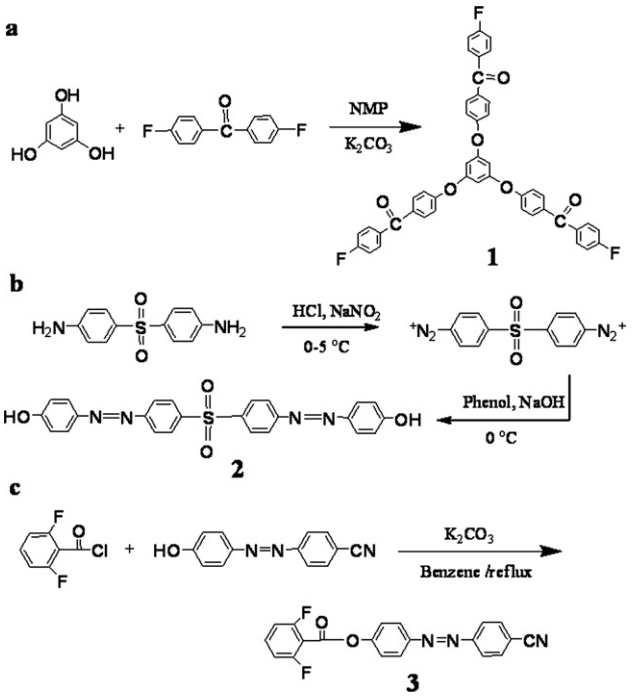

Scheme 2 Synthesis routes to a) monomer **1**, b) monomer **2** and c) monomer **3**.

4,4′-Dihydroxyphenylazodiphenylsulfone (monomer 2, Scheme 2b). Monomer **2** was synthesized by a diazotization reaction followed by coupling with phenol. Into a 1000 mL beaker equipped with a mechanical stirrer, a dropping funnel, and a thermometer were placed water (50 mL), ice (50 mL) and DDS (24.8 g, 0.1 mol). Hydrochloric acid (0.8 mol, 67.2 mL) was added drop-wise into the stirred mixture through the dropping funnel. The solution was cooled to 0–5 °C in an ice-water bath and then a concentrated water solution of sodium nitrite (13.8 g, 0.2 mol) was added drop-wise. The mixture was stirred for 30 min at 0–5 °C, and yielded a clear solution. The resulting solution was filtered and added drop-wise into a solution of NaOH (8.0 g, 0.2 mol), phenol (18.8 g, 0.2 mol), and sodium bicarbonate (25.2 g, 0.3 mol) in 100 mL water. The reaction mixture was stirred at 0–5 °C for about 2 h and then at room

temperature for another 2 h. The final solution was added slowly to 700 mL acid water (HCl) and a brown–orange precipitate of the azo-compound was formed. The precipitate was collected by filtration, and washed thoroughly with water containing a little amount of sodium hydrogen carbonate (pH = 8). The solid was dried at 60 °C in a vacuum oven and finally recrystallized from a mixture of THF and ethanol to obtain a pure orange–yellow powder (60% yield). m.p ~288 °C (decomp.); *m/z* (MALDI-TOF): 459 (M^+ + H, $C_{24}H_{18}N_4SO_4$ requires 458.10). ν_{max}/cm^{-1} 3393 (–OH), 3048 (Ar–H), 1294 (–SO_2–), 1263, 1140 (–SO_2–); δ_H (500 MHz; $CDCl_3$, Me_4Si): 10.54 (2H, s, –OH), 8.17 (4H, d, J = 8.6 Hz, ArH), 7.98 (4H, d, J = 8.6 Hz, ArH), 7.86 (4H, d, J = 8.9 Hz, ArH), 6.96 (d, 4H, J = 8.9 Hz, ArH); δ_c (125 MHz; $CDCl_3$, Me_4Si): 162.57, 155.41, 145.80, 141.81, 129.33, 126.06, 123.50, 116.75; Calculated C, 62.87; H, 3.96; N, 12.12; O, 13.96; Found C, 63.05; H, 3.77; N, 12.35; O, 13.77.

4-((4-Cyanophenyl)diazenyl)phenyl-2,6-difluorobenzoate (monomer 3, Scheme 2c). Monomer **3**, an azo-bisfluoro monomer, was synthesized according to our previously reported procedure.[24b] (85% yield); m.p. 194 °C; *m/z* (MALDI-TOF): 364.5 (M^+ + H, $C_{20}H_{11}F_2N_3O_2$ requires 363.08). ν_{max}/cm^{-1} 3030 (Ar-H), 2234 (–CN), 1754 (–CO–O–), 1012 (–C–F). δ_H (500 MHz; $CDCl_3$, Me_4Si): 8.05 (2H, d, J = 8.8 Hz, ArH), 8.00 (2H, d, J = 8.4 Hz, ArH), 7.83 (2H, d, J = 8.4 Hz, ArH), 7.54 (1H, s, ArH), 7.46 (2H, d, J = 8.8 Hz, ArH), 7.06 (2H, t, J = 8.2 Hz, ArH). δ_c (125 MHz; $CDCl_3$, Me_4Si): 162.1, 160.0, 154.4, 153.2, 150.3, 133.8, 133.4, 124.7, 123.4, 122.5, 120.6, 118.4, 114.2, 112.4.

Azo-HPAE 4a (Scheme 3). A 75 mL three-necked flask equipped with a mechanical stirrer, a Dean–Stark trap, a cold water condenser, an N_2 inlet/outlet and a thermometer was charged with monomer **1** (1.80 g, 2.5 mmol), 4,4′-dichlorodiphenyl sulfone (0.72 g, 2.5 mmol), monomer **2** (0.85 g, 1.85 mmol), BPA (0.42 g, 1.85 mmol), K_2CO_3 (0.54 g, 3.86 mmol), tetramethylene sulfone (TMS, 20 mL) and toluene (15 mL). The reaction mixture was refluxed at 120 °C for 2 h under N_2 atmosphere to dehydrate the system. After dehydration and removal of toluene, the reaction temperature was then increased to 140 °C and maintained at this temperature for 12 h until a viscous solution was obtained. Then the viscous solution was slowly poured into 500 mL water and the threadlike polymer was obtained. After pulverized into powders, the polymer was washed with hot deionized water and extracted in a Soxhlet extractor with alcohol. The resulting product was dried at 100 °C under vacuum for 24 h and **4a** was obtained as red solid (85% yield). ν_{max}/cm^{-1} 3056 (Ar-H), 2969 (–CH_3), 1659 (C=O), 1235 (Ar–O–Ar). δ_H (500 MHz; $CDCl_3$, Me_4Si): 8.20–8.05 (m, ArH), 7.91–8.05 (m, ArH), 7.67–7.91 (m, ArH), 7.35–6.85 (m, ArH), 6.59 (s, ArH), 1.68 (s, –CH_3); GPC: number-average molecular weight (M_n) 5.6 × 10^3; polydispersity (M_w/M_n) 1.70.

Azo-HPAE 4b (Scheme 3). The synthesis was carried out following the same procedure described for **4a**, but using monomer **1** (1.8025 g, 2.5 mmol), monomer **3** (0.91 g, 2.5 mmol), BPA (0.84 g, 3.7 mmol), K_2CO_3 (0.54 g, 3.86 mmol), TMS (20 mL) and toluene (15 mL). After purification, an orange solid of **4b** was obtained (90% yield). ν_{max}/cm^{-1} 3030 (Ar-H), 2969 (–CH_3), 2223 (–CN), 1750 (–CO–O–), 1659 (–C=O), 1234 (–Ar–O–Ar–). δ_H (500 MHz; $CDCl_3$, Me_4Si): 8.05–7.90 (m, ArH), 7.89–7.70 (m, ArH), 7.24–6.80 (m, ArH), 6.65–6.55 (s, ArH), 1.68 (s, –CH_3); GPC: number-average molecular weight (M_n) 1.3 × 10^4; polydispersity (M_w/M_n) 2.03.

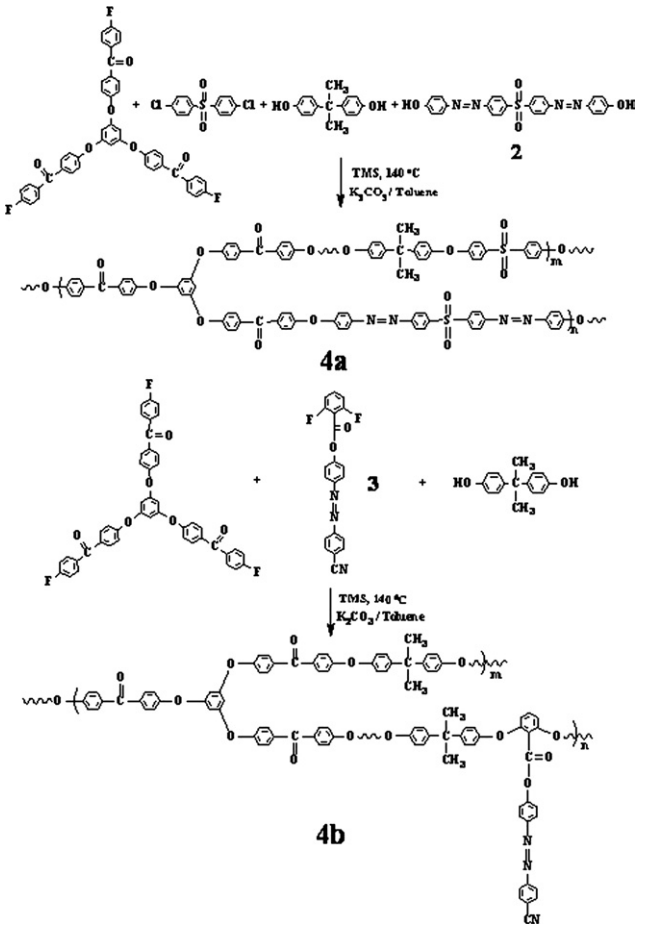

Scheme 3 Synthesis routes to azo-HPAEs **4a** and **4b**.

Preparation of polymer films

Polymers were dissolved in cyclohexanone (10 wt%) and then filtered through 0.8 μm syringe filters membranes. Polymer films were obtained by spin coating (for SRG) or casting (for birefringence) the polymer solution onto glass substrates, which were cleaned in the ultrasonic bath with DMF, THF, ethanol and distilled water subsequently. The thickness of the films was controlled to be about 0.5–1.0 μm by adjusting the spinning rate for fabricating SRG and the thickness of the casting films were about 8–10 μm for the photoinduced birefringence experiment. The residual solvent was removed by heating the films in a vacuum oven at 100 °C for 2 days. The films were stored in a desiccator for further studies.

Results and discussion

Monomer synthesis and characterization

The 'core' molecule B_3 (monomer **1**) was synthesized by nucleophilic substitution of excess 4,4′-difluorobenzophenone with phloroglucinol in the presence of K_2CO_3. The structure of

monomer **1** is shown in Scheme 2a and confirmed by MS, IR and ^{1}H NMR. The IR spectrum shows the characteristic bands of –C=O and –O– stretching vibrations at 1656 and 1238 cm^{-1}, respectively. We prepared a new bisphenol (monomer **2**) containing azo groups by a diazotization reaction, as shown in Scheme 2b. The structure of **2** is confirmed by MS, IR, UV-visible and ^{1}H NMR spectroscopy. The IR spectrum exhibits a characteristic band of –OH at 3393 cm^{-1}. UV-vis absorptions of monomer **2** are at 376 and 470 nm, and they are assigned to $\pi \rightarrow \pi^*$ and $n \rightarrow \pi^*$ electronic transitions of azo-aromatic chromophores, respectively. In the ^{1}H NMR spectrum of monomer **2**, all of the signals are well within agreement with the expected structure. The signal at 10.54 ppm in the ^{1}H NMR is assigned to the hydroxyl proton.

Polymer synthesis and structure characterization

Azo-HPAEs were synthesized by using $B_3 + A_2$ methodology *via* a typical nucleophilic substitution polycondensation reaction with 1,3,5-tris(4-(4-fluorobenzoyl)phenoxy)benzene as a B_3 'core' molecule (Scheme 3). Prepared hyperbranched polymers with $B_3 + A_2$ monomers is a novel method developed by Jikei *et al.*, Fréchet *et al.*, and Long *et al.*[25–27] One advantage of this approach is that the performance of polymer can be mediated by adjusting the structure and chain length of B_3 or A_2. Furthermore, performing direct polycondensation close to the gel point makes the structure of the polymer's aggregation state also controllable. However, the solubility of the resulting polymer of B_3 and A_2 is very poor, and not suitable for fabrication of the casting films. By introduction of the additional monomers, the solubility of the copolymers can be improved greatly and qualified for fabrication of the casting films. Two branched copolymers, azo-HPAEs **4a** and **4b**, were designed as synthesized according to Scheme 3. Since the reactive groups of the monomers have no selectivity and both the bis-phenol monomers could react with monomer **1** and 4,4′-dichlorodiphenyl sulfone (for **4a**) or monomer **3** (for **4b**) optionally. Thus, the real structure of azo-HPAEs **4a** and **4b** may be more complicated than that shown in Scheme 3. However, it is difficult to give out the real structure of the resulting random copolymers due to complexity of the reactions. Therefore, we represent the three branches of azo-HPAEs **4a** and **4b** with different lengths, as shown in Scheme 1.

As shown in Table 1, both the resulting azo-HPAEs, **4a** and **4b**, have a inherent viscosity of 0.29 dL g^{-1} in DMF at 25 °C, indicating their low inherent viscosity (in comparison with their linear analogues). Although the number-average molecular weight (M_n) of **4a** and **4b** were only 5.6×10^3 ($M_w/M_n = 1.70$) and 1.3×10^4 ($M_w/M_n = 2.03$), the real molecular weight of the polymers may be even larger than the values referred to polystyrene standards because dendritic macromolecules generally have a smaller size than linear polymers with the same molecular weight and can hardly be expanded in solution. The broad molecular weight distribution should be ascribed to the specific characteristics of the nucleophilic substitution polycondensation reaction of $B_3 + A_2$. The polymers of azo-HPAEs are well soluble in various solvents such as chloroform, THF, DMF, DMSO, NMP and cyclohexanone, but insoluble in acetone and ethanol.

The chemical structures of azo-HPAEs were confirmed by IR, ^{1}H NMR and UV-vis spectra. The IR spectra of **4a** and **4b** are shown in Fig. 1. In the IR spectrum of **4a**, the absorption bands at 2969, 1659 and 1234 cm^{-1} are attributed to the stretching vibrations of the methyl (–CH_3), diphenylcarbonyl (–C=O) and the aromatic ether group (Ar–O–Ar), respectively. In the IR spectrum of **4b**, two additional characteristic absorption bands at 2223 and 1750 cm^{-1} attributed to the nitrile (–CN) stretching vibration and the carbonyl stretching vibration of the conjugated carboxylic esters (–*CO*–O–) could be identified. Fig. 2 shows the signal assignments of the ^{1}H NMR spectra of the azo-HPAEs **4a** and **4b** in $CDCl_3$. Although the signals in the ^{1}H NMR spectra of azo-HPAEs are complicated and greatly overlapped, which make the spectra difficult to analyze, the signals corresponding to the protons of –CH_3 (δ, 1.68), the protons located at *ortho*-position of –phloroglucinol–O–Ph– group (δ, 6.59), azo (–*Ph*–N=N–*Ph*–) group (δ, 7.97) and –N=N–*Ph*–SO_2–*Ph*–N=N– (δ, 8.11) are distinguished from other protons. UV-visible spectra of **4a**

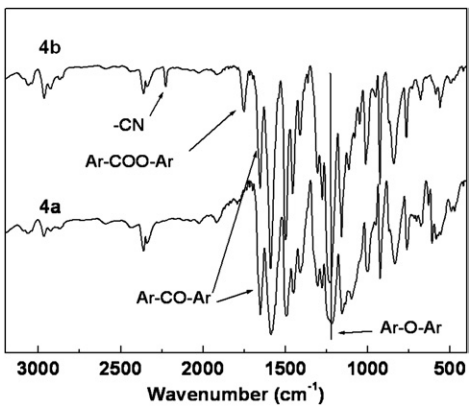

Fig. 1 IR (KBr) spectra of azo-HPAEs **4a** and **4b**.

Table 1 Properties of azo-HPAEs **4a** and **4b**

Polymer	η_{iv}[a]/dL g^{-1}	T_g[b]/°C	DT_5[c]/°C[d]		DT_{10}[c]/°C[e]		M_n	M_w/M_n
			Air	N_2	Air	N_2		
4a	0.29	150	422	405	461	442	5.6×10^3	1.70
4b	0.29	143	429	423	469	466	1.3×10^4	2.03

[a] Inherent viscosity was determined on an Ubbelohde viscometer in a thermostatic container with the polymer concentration of 0.5 g dL^{-1} in DMF at 25 °C. [b] Glass transition temperature from DSC. [c] DT = decomposition temperature. [d] 5% weight-loss temperatures were detected at a heating rate of 10°C min^{-1} in nitrogen or air with a gas flow of 100 mL min^{-1}. [e] 10% weight-loss temperatures were detected at a heating rate of 10°C min^{-1} in nitrogen or air with a gas flow of 100 mL min^{-1}.

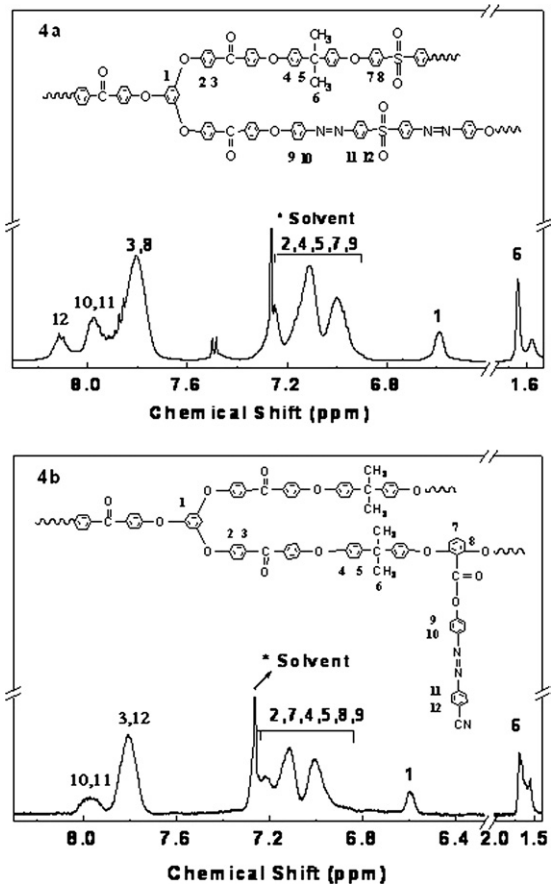

Fig. 2 ^{1}H NMR spectra of azo-HPAEs **4a** and **4b** in $CDCl_3$.

and **4b** in DMF solutions and as spin-coating thin films are given in Fig. 3. From the spectra, we could see the characteristic absorption bands of $\pi \rightarrow \pi^*$ and $n \rightarrow \pi^*$ electronic transitions of azo-aromatic chromophores in the range of 300–500 nm. Compared with the maximum absorption (λ_{max}) of **4a** and **4b** in the DMF solutions appeared at 359 and 351 nm, the λ_{max} of the corresponding films spectra experience a red-shift to 362 and 355 nm, contributed to the solvatochromism effect of the internal azo-chromophores when the environments of the polymeric

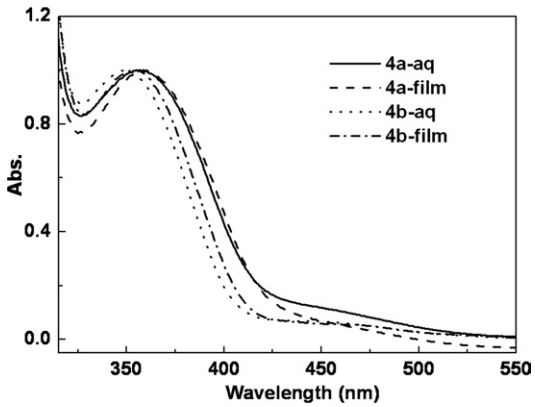

Fig. 3 UV-vis absorption spectra of azo-HPAEs **4a** and **4b** in DMF solutions and as spin-coated films at room temperature.

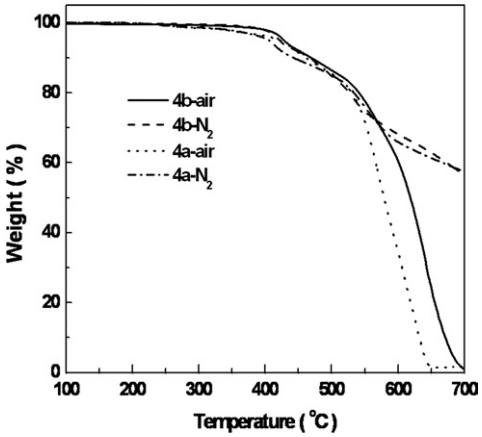

Fig. 4 TGA curves of azo-HPAEs **4a** and **4b** in nitrogen and in air.

chains changed from solutions to solid films. All of the above results obtained from IR, ^{1}H NMR and UV-vis spectra indicate that the designed hyperbranched azo-polymers are successful synthesized.

Thermal properties and morphologies of azo-HPAEs

TGA curves of the azo-HPAEs are given in Fig. 4 and the detailed experimental data are illustrated in Table 1. The TGA thermograms of **4a** and **4b** indicate that their 5% weight loss temperatures are all above 400 °C in both air and nitrogen gas, indicating the excellent thermal stability of azo-HPAEs **4a** and **4b**. T_g values of azo-HPAEs were determined by differential scanning calorimetry (DSC). In the curves, the hyperbranched polymers **4a** and **4b** show the second-order phase transition and no other thermo changes except that glass transitions are observed below the decomposition temperatures, indicating the amorphous nature of azo-HPAEs **4a** and **4b**. Due to the aromatic structure and the large dipole moment of the side groups, **4a** and **4b** show high glass transition temperatures, which ensured their excellent thermal property. The glass transition temperatures (T_g) of the polymers obtained by DSC are also listed in Table 1.

The wide-angle X-ray diffractions of **4a** and **4b** are shown in Fig. 5. The curves of azo-HPAEs are broad and without obvious peak features, which also indicate their amorphous character.

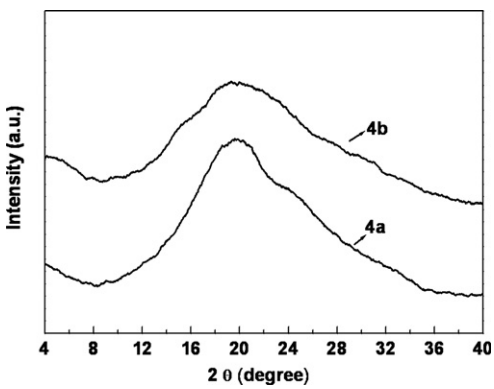

Fig. 5 Powder WAXD patters of **4a** and **4b** at room temperature.

Photochromic behavior of azo-HPAEs

The UV-vis absorption spectrum of **4b** in DMF solution exhibits two absorption bands centered around 351 and 447 nm in the range of 300–650 nm, corresponding to $\pi \rightarrow \pi^*$ and $n \rightarrow \pi^*$ electronic transitions of azo-aromatic chromophores, respectively. The high energy band is mainly attributed to the *trans*-isomer, whereas the low energy one is mainly derived from the metastable *cis*-isomer. When the solution was irradiated by light of 360 nm, azobenzene chromophores undergo a *trans*-to-*cis* photoisomerization process (Fig. 6a). The absorption band at 351 nm decreases gradually and the absorption band at 447 nm increases gradually with the prolonged irradiation time. The photostationary state of the photoisomerization is reached after irradiation for 300 s. On the other hand, when the irradiated sample was annealed at a certain temperature or irradiated with visible light, the absorption peak at 351 nm will gradually recover to the starting value before irradiation (Fig. 6b), confirming the reversibility of the photoisomerization process. The proportion of isomerization at the photostationary state can be estimated from eqn 1:

$$\Phi = 100(1 - A_t/A_0)\ \% \quad (1)$$

where A_0 and A_t are the absorptions at the maximum before and after irradiation, respectively. The hyperbranched polymer **4a** also shows the same reversibility of the photoisomerization process. This result clearly indicates the homogeneous photochromic behavior for *trans*- and *cis*-azobenzene chromophores in the polymer samples. From the experiments, the proportions of isomerization at the photostationary state of **4a** and **4b** are determined to be 21.1 and 50.6%, respectively. Such a difference might come from the fact that it is more difficult for the azobenzene groups to change from *trans*- to *cis*- when they are attached to the polymer main chain.

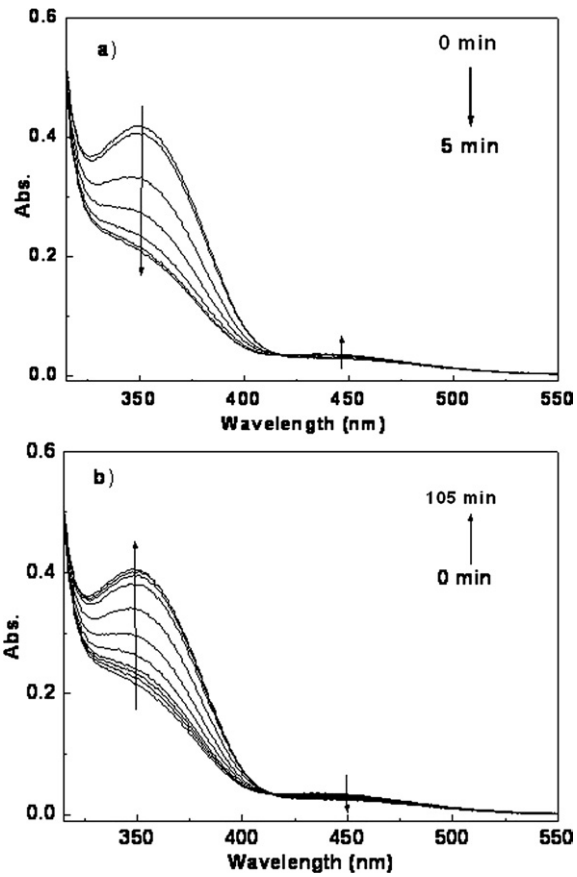

Fig. 6 Changes in the UV-vis absorption spectra of **4b** in DMF solution at 25 °C with different irradiation time under (a) 360 nm light irradiation and (b) visible light irradiation.

Preparation and characterization of surface-relief gratings

Formation of photoinduced surface-relief gratings (SRGs) is one of the most interesting properties of azo-polymers in recent years.[2,10,11,20,21] By exposure of the polymer films to the interfering laser beams, SRGs will be formed on the films at a temperature well below the T_g of the samples. This function could be potentially applied to holographic memories, reversible optical data storage and waveguide couplers.

The experimental setup for the surface-relief gratings formation is shown in Fig. 7. A polarized Nd:YAG nanosecond pulsed UV laser beam (Spectra-Physics, Quanta-Ray-150, 355 nm), with pulse duration of 10 ns and repetition rate of 10 Hz, was used as the light source. The spot of the laser beam is 10 mm in diameter, and the intensity of the recording laser conforms to a Gauss distribution. Surface-relief gratings were optically inscribed on the spin-coating films with polarized interfering laser beams, where the laser beam was split by beam splitting (BS) and the reflected half-beam coincided with the other half on the film surface. The surface profiles of the resulting gratings were observed using an atomic force microscope (AFM) in the tapping mode.

It is interesting to have found that SRGs of **4a** and **4b** could be rapidly fabricated within 30 s at room temperature with a modest intensity (about 60 mW cm^{-2}). Fig. 8 shows the typical AFM plane and three-dimensional images of the surface structures. The gratings profile of **4a** and **4b** exhibit the same regularly sinusoidal shapes with grating spacings of ~1.6 μm, as set by the interference pattern. From the AFM measurement, the surface modulation depths of **4a** and **4b** are about 145 and 100 nm, respectively. In addition, the modulation depth could be well adjusted by the irradiation time and the irradiation energy. The spatial period depend on both the angle (θ) between the two interfering beams and the wavelength (λ) of the writing beams.

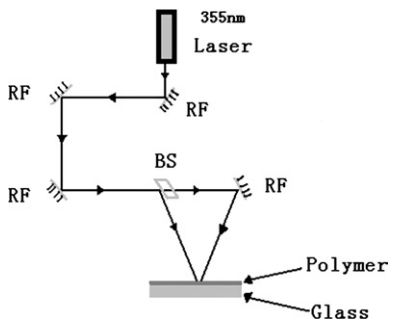

Fig. 7 Experimental setup for SRGs inscription. (BS = beam splitting; RF = flector).

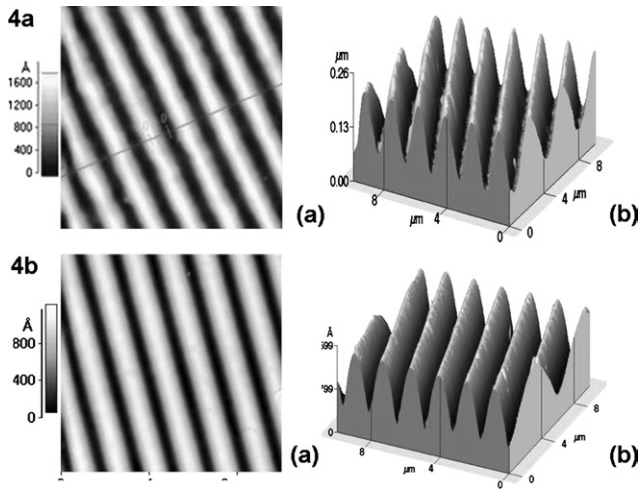

Fig. 8 AFM images of the SRGs formed on azo-HPAEs **4a** and **4b** films. (a) The plane view of the SRGs (the image size is 10 × 10 μm). (b) Typical 3-D view of the SRGs.

Another important requirement of a SRGs is the shape stability in terms of long-term storage and durability at higher temperatures.[21,28,29] To test whether the SRGs based on such hyperbranched polymers could withstand high temperature, we observed the changes of the surface profiles of the films from 25 to 300 °C at a heating rate of 10 °C min^{-1} by polarized optical microscope (POM) with a Linkam THMS 600 hot stage. The azo-HPAEs **4a** and **4b** films could keep good stability at 200 °C. Surface-relief gratings of the films of **4b** became blurry when they were heated to 220 °C and then evidently removed at 260 °C. In contrast to SRGs of **4b**, the induced inscriptions on **4a** films are only partially erasable by thermal treatment and kept good stability at the temperature of 260 °C. The gratings of **4a** could not be totally erased by heating, even at 300 °C. The morphologies of the film surfaces after heating were also observed by AFM. Fig. 9 shows the AFM images of **4a** and **4b** films after heating to 300 °C. Clearly, in the **4a** film, the SRGs structure could be still kept pretty well after the thermal treatment and the amplitude of the remaining reliefs is about 120 nm. But for **4b**, most of the SRGs are removed and the amplitude of the reliefs remained is only about 10 nm. It is concluded that both the SRGs of the hyperbranched polymer **4a** and **4b** films have good thermal shape stability and the main chain type azo-polymer **4a** shows even better persistent fixation than the side chain type azo-polymer **4b**.

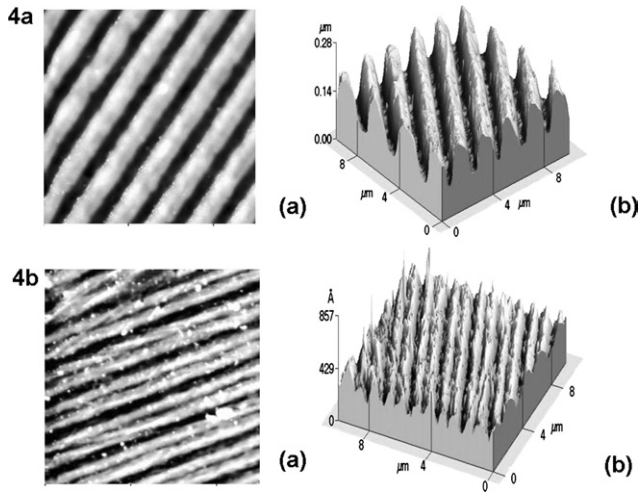

Fig. 9 AFM images of the SRCs on **4a** and **4b** films after heating treatment. (a) Plane (10 × 10 μm) and (b) typical 3-D view of the SRGs.

Photoinduced birefringence

Birefringence measurements were produced by a pump beam (532 nm of Nd:YAG laser) polarized at 45° with respect to the polarization of the probe beam (632.8 nm He:Ne laser). The samples were placed between two crossed polarizers (P and A) in the path of the probe laser beam. The transmitted probe beam was detected by a photo detector and connected through a lock-in amplifier to a computer. The probe light was modulated at 980 Hz by a mechanical chopper. A birefringence $\triangle n$ induced by 532 nm pump laser resulted in transmission of the 632.8 nm probe beam through polarizer A. The intensity of this transmitted beam could be described by the well-known eqn 2:[30,31]

$$I_t = I_o \sin^2(\pi \triangle nd/\lambda) \quad (2)$$

where d is the sample's thickness, λ is the probe laser wavelength and I_o is the transmitted probe light intensity when the polarizer and analyzer are parallel to each other and the sample is not exposed to the polarized 532 nm laser light.

Fig. 10 shows the measured photoinduced birefringence of **4a** and **4b** as a function of time. The time at which the pump laser was switched on or off was marked with a letter. From the multiple "writing–erasing" photoinduced birefringence cycles on the films we could see that at the beginning of the experiments, no light is transmitted through the analyzer (0–20 s) due to the random orientation of the azo compounds. When the polarized Nd:YAG laser beam radiation was introduced (marked A in Fig. 10), an anisotropic orientation distribution is expected as a consequence of the accumulation of the azo chromophores that are oriented perpendicular to the polarization vector of the writing beam. Light is thus transmitted through the analyzer due

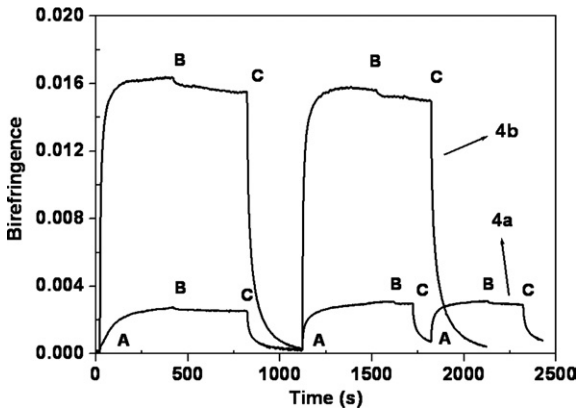

Fig. 10 Multiple 'writing–erasing' photoinduced birefringence on the films of azo-HPAEs **4a** and **4b** at room temperature. At point A the linearly polarized laser ('writing' beam) was on; at point B the linearly polarized laser was switched off; at point C the circularly polarized laser ('erasing' beam) was on.

to the onset of birefringence. When the excitation light was turned off (B in Fig. 10), the birefringence value exhibits a little decay and then reaches a stable state in a few minutes. This result might be mainly caused by the thermal reorientation of some azobenzene groups and the interactions of orientated azobenzene groups on a long-term basis. Compared with other azo-polymers,[11b, 32–35] azo-HPAEs show smaller birefringence decay and possess a remnant birefringence larger than 90% of the initial value, indicating that these polymers present improved stability in the case of the photoinduced orientation. This is mainly attributed to the high glass transition temperatures and rigid aromatic structure of azo-HPAEs, which limit the relaxation process of the oriented chromophore groups. At a third stage in the writing sequence (C in Fig. 10), the optically induced birefringence is thoroughly "erased" by overwriting the test spot with circularly polarized Nd:YAG laser beam, suggesting the randomized orientation of the azobenzene groups. Finally, when the writing beam was turned on again (A in Fig. 10), reorientation occurred. Both of the films of **4a** and **4b** could be written and erased repeatedly.

Although **4b** bears fewer azobenzene chromophores than **4a**, the birefringence signal intensity of **4b** is five times of that of **4a** at the saturation state. Under the same experiment conditions outline above, $\triangle$n reaches the saturation values higher than 0.003 for **4a** and 0.015 for **4b** within several minutes, respectively. This might be due to the different locations of the substitute azo moieties in the hyperbranched architectures. The chromophores in polymer **4a** (with azo moieties in the main chains of the branched arms) are difficult to be oriented compared to those in **4b** (with azo moieties in the side chains of the branched arms).

Conclusions

Novel hyperbranched azo-poly(aryl ether)s **4a** and **4b** prepared by $B_3 + A_2$ methodology exhibit high T_g, good thermal stability and homogeneous photochromic behaviors. They are qualified for rapid fabrication of thermally stable surface relief gratings. The polymer with azobenzene moieties in the side chain presents larger and better reversible photoinduced birefringence than the one with azobenzene moieties in the main chain upon irradiation with 532 nm Nd:YAG laser. The hyperbranched azo-polymers are expected to be promising materials with application potentials in holographic memories, reversible high density optical storage, optical switch, and other photo-driven devices.

References

1 (*a*) Z. Z. Stephan and H. Dietrich, *Adv. Mater.*, 1998, **10**, 855–859; (*b*) A. Natansohn and P. Rochon, *Chem. Rev.*, 2002, **102**, 4139–4175; (*c*) A. S. Matharu, S. Jeeva, P. R. Huddleston and P. S. Ramanujam, *J. Mater. Chem.*, 2007, **17**, 4477–4482; (*d*) Y. B Li, Y. N. He, X. L. Tong and X. G. Wang, *J. Am. Chem. Soc.*, 2005, **127**, 2402–2403.

2 (*a*) S. W. Cha, D. H. Choi and J. I. Jin, *Adv. Funct. Mater.*, 2002, **12**, 670–678; (*b*) E. Ishow, B. Lebon, Y. N. He, X. G. Wang, L. Bouteiller, L. Galmiche and K. Nakatani, *Chem. Mater.*, 2006, **18**, 1261–1267.

3 L. L. Beth, A. M. Stefan and A. A. Hanrry, *Adv. Mater.*, 2004, **16**, 1746–1750.

4 (*a*) H. Rainer and B. Thomas, *Adv. Mater.*, 2001, **13**, 1805–1810; (*b*) Z. A. Li, Z. Li, C. A. Di, Z. C. Zhu, Q. Q. Li, Q. Zeng, K. Zhang, Y. Q. Liu, C. Ye and J. G. Qin, *Macromolecules*, 2006, **39**, 6951–6961; (*c*) Q. Zeng, Z. A. Li, Z. Li, C. Ye, J. G. Qin and B. Z. Tang, *Macromolecules*, 2007, **40**, 5634–5637.

5 (*a*) Y. L. Yu, M. Nakano and T. Ikeda, *Nature*, 2003, **425**, 145–145; (*b*) Y. L. Yu and T. Ikeda, *Angew. Chem., Int. Ed.*, 2006, **45**, 5416–5418.

6 T. Todorov, P. Markovski, N. Tomova, V. Dragostinova and K. Stoyanova, *Opt. Quantum Electron.*, 1984, **16**, 471–476.

7 T. Ikeda and O. Tsutsumi, *Science*, 1995, **268**, 1873–1875.

8 K. Ichimura, S. K. Oh and M. Nakagawa, *Science*, 2000, **288**, 1624–1626.

9 T. Hugel, N. B. Holland, A. Cattani, L. Moroder, M. Seitz and H. E. Gaub, *Science*, 2002, **296**, 1103–1106.

10 P. Rochon, E. Batalla and A. Natansohn, *Appl. Phys. Lett.*, 1995, **66**, 136–138.

11 (*a*) D. Y. Kim, S. K. Tripathy, L. Li and J. Kumar, *Appl. Phys. Lett.*, 1995, **66**, 1166–1168; (*b*) C. Chun, M. Kim, D. Vak and D. Y. Kim, *J. Mater. Chem.*, 2003, **13**, 2904–2909.

12 S. Xie, A. Natansohn and P. Rochon, *Chem. Mater.*, 1993, **5**, 403–411.

13 (*a*) D. Junge and D. McGrath, *Chem. Commun.*, 1997, **9**, 857–858; (*b*) D. Junge and D. McGrath, *J. Am. Chem. Soc.*, 1999, **121**, 4912–4913.

14 A. Sidorenko, C. Houphouet-Boigny, O. Vilavicencio, M. Hashemzadeh, D. McGrath and V. Tsukruk, *Langmuir*, 2000, **16**, 10569–10572.

15 J. A. Delaire and K. Nakatani, *Chem. Rev.*, 2000, **100**, 1817–1845.

16 X. Li, X. M. Lu, Q. H. Lu and D. Y. Yan, *Macromolecules*, 2007, **40**, 3306–3312.

17 R. Alcala, R. Gimenez, L. Oriol and M. Pinol, *Chem. Mater.*, 2007, **19**, 235–246.

18 (*a*) T. Nagasaki, S. Tamagaki and K. Ogino, *Chem. Lett.*, 1997, **8**, 717–718; (*b*) S. Yokoyama, T. Nakahama, A. Otomo and S. Mashiko, *J. Am. Chem. Soc.*, 2000, **122**, 3174–3181; (*c*) T. Aida and D. Jiang, *Nature*, 1997, **388**, 454–456; (*d*) S. Yokoyama, T. Nakahama, A. Otoma and S. Mashiko, *Thin Solid Films*, 1998, **331**, 248–253.

19 (*a*) Z. Li, A. J. Qin, J. W. Y. Lam, Y. P. Dong, C. Ye, I. D. Williams and B. Z. Tang, *Macromolecules*, 2006, **39**, 1436–1442; (*b*) C. Gao and D. Y. Yan, *Prog. Polym. Sci.*, 2004, **29**, 183–275; (*c*) M. Jikei and M. Kakimoto, *Prog. Polym. Sci.*, 2001, **26**, 1233–1285; (*d*) K. Inoue, *Prog. Polym. Sci.*, 2000, **25**, 453–571; (*e*) Z. C. Zhu, Z. A. Li, Y. Tan, Z. Li, Q. Q. Li, Q. Zeng, C. Ye and J. G. Qin, *Polymer*, 2006, **47**, 7881–7888.

20 (*a*) Y. N. He, X. G. Wang and Q. X. Zhou, *Synth. Met.*, 2003, **132**, 245–248; (*b*) P. C. Che, Y. N. He and X. G. Wang, *Macromolecules*, 2005, **38**, 8657–8663.

21 (*a*) N. Zettsu, T. Ubukata, T. Seki and K. Ichimura, *Adv. Mater.*, 2001, **13**, 1693–1697; (*b*) H. Nakano, T. Tanino, T. Takahashi, H. Ando and Y. Shirota, *J. Mater. Chem.*, 2008, **18**, 242–246.

22 (*a*) H. B. Zhang, J. H. Pang and Z. H. Jiang, *J. Membr. Sci.*, 2005, **264**, 56–64; (*b*) Y. Gao, G. P. Robertson, M. D. Guiver, S. D. Mikhailenko and S. Kaliaguine, *Macromolecules*, 2005, **38**, 3237–3245; (*c*) X. Y. Ma, Z. H. Lv, D, Wang and Z. H. Jiang, *J. Photochem. Photobiol., A*, 2007, **188**, 43–50.

23 G. X. Jiang, B. Yao and L. X. Wang, *Macromolecules*, 2006, **39**, 1403–1409.

24 (*a*) Z. Q. Lu, P. Shao and J. G. Qin, *Macromolecules*, 2004, **37**, 7089–7096; (*b*) X. B. Chen, J. J. Zhang and Z. H. Jiang, *Dye and Pigments*, 2008, **77**, 223–228.

25 J. J. Hao, M. Jikei and M. A. Kakimoto, *Macromolecules*, 2003, **36**, 3519–3528.

26 T. Emrick, H. Chang and J. Fréchet, *Macromolecules*, 1999, **32**, 6380–6382.

27 M. G. McKee, T. Park, S. Unal and T. E. Long, *Polymer*, 2005, **46**, 2011–2015.

28 T. Fukuda, H. Matsuda, T. Shiraga, T. Kimura, M. Kato, N. K. Viswanathan, J. Kumar and S. K. Tripathy, *Macromolecules*, 2000, **33**, 4220–4225.

29 J. Gao, Y. N. He, H. P. Xu, B. Song, X. Zhang, Z. Q. Wang and X. G. Wang, *Chem. Mater.*, 2007, **19**, 14–17.

30 S. P. Bian and S. K. Tripathy, *Adv. Mater.*, 2000, **12**, 1202–1205.

31 T. Todorov, L. Nikalava and N. Tomova, *Appl. Opt.*, 1984, **23**, 4309–4312.

32 R. Fernandez, I. Mondragon, P. A. Oyanguren and M. J. Galante, *React. Funct. Polym.*, 2008, **68**, 70–76.

33 Y. Wu and A. Natansohn, *Macromolecules*, 2001, **34**, 7822–7828.

34 A. Natansohn and A. Hay, *Chem. Mater.*, 1995, **7**, 1612–1615.

35 S. W. Cha and D. H. Choi, *Adv. Funct. Mater.*, 2001, **11**, 355–360.

